Journal of Materials Chemistry A

PAPER

View Article Online
View Journal | View Issue

CrossMark click for updates

Cite this: J. Mater. Chem. A, 2016, 4, 13228

Energy storage systems based on endoskeleton structuring†

Inho Nam,‡ Jongseok Park, Seongjun Bae, Soomin Park,§ Young Geun Yoo and Jongheop Yi*

Received 5th May 2016
Accepted 27th July 2016

DOI: 10.1039/c6ta03738k

www.rsc.org/MaterialsA

As electronic devices have continued to advance, consistent with Moore's law, it is clear that the development of technology can create new types of products and jobs and even industrial sectors. While human integrated devices, storage of fluctuating energy sources and electric transports are required in the near future, one field of electronics has not fully developed, – *i.e.*, energy storage devices. In order to overcome this impediment, we developed a new approach of energy systems that is inspired by the difference in evolutionary genealogy between animals, *i.e.*, insects (exoskeleton) *versus* vertebrates (endoskeleton). The new energy storage technology proposed here includes an endoskeleton architecture similar to vertebrates, which (1) provides flexibility for future mobile/human integrated electrics, (2) ensures the scalability of devices for the storage of fluctuating energy sources and (3) solves safety issues associated with energy storage devices in electric vehicles.

Introduction

In bio-systems, each step forward in the evolution of new abilities is made possible by further evolution, but at the same time, mechanical and physiological conditions are created that place definite limits on the present conditions and future possibilities for evolution.[1] This evolution limitation, which is explained by Dollo's law, can also be applied to technology innovation. Since the introduction of the first battery as a Volta pile (1800, Volta, A.),[2] energy storage systems have been developed based on external passive structures as an innovative system. The existence of external covers in energy storage devices makes them popular, because the passive scaffolds maintain the structure of a device and minimize dangers that are caused by changes in external forces and the environment.[2] The architecture of energy storage devices, however, has encountered limitations in state of the art electronics, such as (1) limited flexibility, (2) limited device size and (3) heat and gas diffusion problems.[3–5]

In the view of its role and structure, conventional external scaffold systems are similar to exoskeleton systems in arthropods, such as insects. The exoskeletons of insects, a hard external cover, provide good protection against physical attacks including crushing or piercing. In addition, it also functions as a skeleton that maintains the architecture of the organic system within it.[6] However, insects were excluded from the paths of development open to their contemporaries, the vertebrates, where a very different series of opportunities opened up, namely the emergence of an endoskeleton.[6] Here, we propose energy storage devices that include an endoskeleton as an alternative to the conventional systems that are now in use and show that endoskeleton systems have advantages that are distinct from the exoskeleton structure of a conventional system.

As shown in Fig. 1, this study represents the first step toward an opposite branch in the evolution of energy storage devices. The architectures of energy storage devices have been developed sequentially in the forms of cylindrical cells, prismatic cells, and pouch cells, all of which consistently involve external scaffolds as an irreversible innovation.[7] State of the art energy storage devices, in order to gain flexibility or stretchability, even include passive external scaffolds, which means that the deformability of their structures is limited.[8–14] Furthermore, they are devoid of in-depth considerations concerning other directions in innovation. There are some critical features of endoskeletons that are related to living systems. First, the flexibility of the body is intrinsically achievable. Second, endoskeletons occupy a small volume compared to that of exoskeletons. Third, the skin of vertebrates can easily transfer gas and heat. These three features are recognizable by a comparison of elephants and ants. Importantly, the following features: (1) flexibility, (2) large size with negligible passive sources and (3) safety against explosions, are urgent issues in the field of state-of-the-art energy storage devices.

School of Chemical and Biological Engineering, WCU Program of C_2E_2, ICP, Seoul National University, Seoul 08826, Republic of Korea. E-mail: jyi@snu.ac.kr

† Electronic supplementary information (ESI) available. See DOI: 10.1039/c6ta03738k

‡ Present address: Center for Plant Aging Research, Institute of Basic Science (IBS), Daegu 42988, Republic of Korea and Department of Chemistry, Stanford University, Stanford, California 94305, USA.

§ Present address: Department of Chemistry, University of California, Berkeley, California 94705, USA.

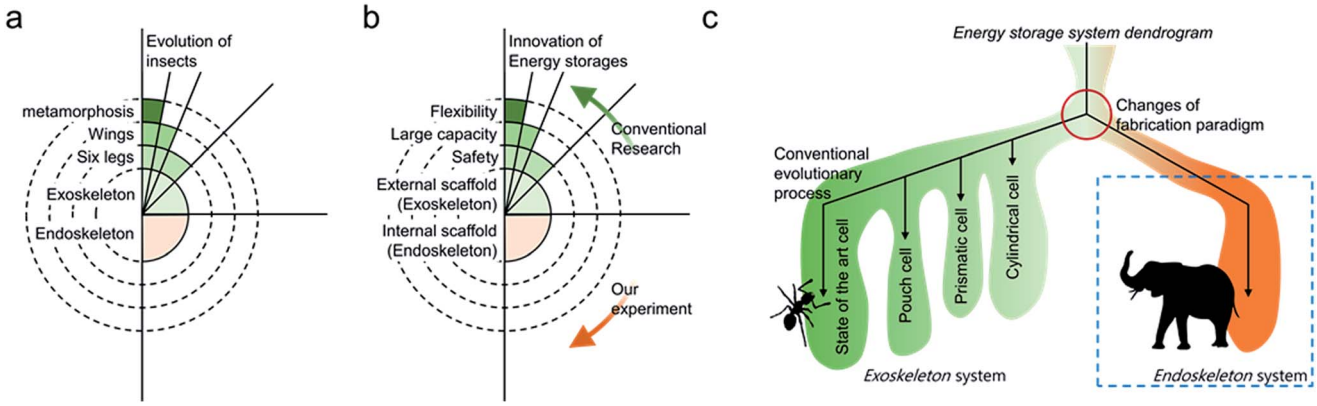

Fig. 1 Branches for the innovation of energy storage systems. (a and b) Progressive reduction in the possibilities of (a) evolution of insects[6] and (b) innovation of energy storage systems. (c) Dendrogram for the innovation of energy storage systems. Opposite branches with changes in the fabrication paradigm are shown.

Experimental section

Endoskeleton energy storage system

CNT inks were prepared by dispersing CNT clusters in ethanol (99.9%) at a concentration of 1 mg ml^{-1} with 30 minutes of ultrasonic treatment. The dispersion was retained for 30 days without any noticeable agglomeration of CNT clusters. Graphene ink was prepared in an analogous manner. The graphene was dispersed and ultrasonically treated in ethanol at the same concentration as the above-mentioned CNT ink. Details of the fabrication of the ink samples can be found in our previous research.[15] CNT ink (1 ml) was poured dropwise onto each side of a polypropylene paper substrate as the internal scaffold and dried, and this step was conducted 20 times. The substrate was placed on a hot plate at a temperature of 313 K for the rapid evaporation of ethanol to uniformly distribute the CNT particles. Graphene nanosheets were deposited on both sides by the same CNT coating method except that the loading amount was 6 mg per side (Fig. S1†). Pores on the cell were patterned into a hexagonal configuration (Fig. S2†). PVA–H_3PO_4 GPE was also prepared as described in a previous report.[16–18] PVA powder (5 g) was dispersed in 40 ml of water with sufficient stirring, and 2.4 ml of H_3PO_4 (85%) was then added to the dispersion. The sample was then heated at 75 °C until it became a transparent gel. Approximately 12 h were needed for the viscous gel to solidify into a thin film with fine flexibility and stretchability. The film was attached to both sides of the as-prepared cell as an external cover.

Finite elemental method (FEM) calculation

Three-dimensional FEM simulations were conducted for numerical structure and transient thermal analyses. Almost all elements of the models were designed by means of a 20-node (serendipity) hexahedral brick. We used an element size under 100 μm for high accuracy.

From Hooke's law, the stress (σ) and strain (ε) of materials are derived as:

$$\sigma_i = D_{ij} \times \varepsilon_i \quad (1)$$

where D_{ij} is the elasticity matrix, which is determined by the following equation.

$$D_{ij} = \frac{E(1-\nu)}{(1+\nu)(1-2\nu)} \begin{bmatrix} 1 & \gamma & \gamma & 0 & 0 & 0 \\ \gamma & 1 & \gamma & 0 & 0 & 0 \\ \gamma & \gamma & 1 & 0 & 0 & 0 \\ 0 & 0 & 0 & \beta & 0 & 0 \\ 0 & 0 & 0 & 0 & \beta & 0 \\ 0 & 0 & 0 & 0 & 0 & \beta \end{bmatrix},$$

$$\sigma_i = \begin{bmatrix} \sigma_{xx} \\ \sigma_{yy} \\ \sigma_{zz} \\ \sigma_{xy} \\ \sigma_{yz} \\ \sigma_{zx} \end{bmatrix}, \varepsilon_i = \begin{bmatrix} \varepsilon_{xx} \\ \varepsilon_{yy} \\ \varepsilon_{zz} \\ \varepsilon_{xy} \\ \varepsilon_{yz} \\ \varepsilon_{zx} \end{bmatrix} \quad (2)$$

where $\gamma = \nu/(1-\nu)$, $\beta = (1-2\nu)/2(1-\nu)$, E is Young's modulus, and ν is Poisson's ratio. The E value of the polypropylene paper appears in the main text. Poisson's ratio is 0.3.

The transient three-dimensional conductive heat transfer equation is:

$$\rho C_P \frac{\partial T}{\partial t} = \frac{\partial}{\partial x}\left(k\frac{\partial T}{\partial x}\right) + \frac{\partial}{\partial y}\left(k\frac{\partial T}{\partial y}\right) + \frac{\partial}{\partial z}\left(k\frac{\partial T}{\partial z}\right) + Q \quad (3)$$

where ρ is the density, C_P is the heat capacity, k is the thermal conductivity and Q is the heat-generation rate per unit volume (here, the surface temperature of electrode is 323 K as a constant). At the boundaries, the heat transfer is expressed by:

$$Q = h(T_s - T_\infty) \quad (4)$$

where h is the convective heat transfer coefficient (30 W m^{-2} K^{-1}, air), T_s is the surface temperature and T_∞ is the ambient temperature (298 K). The ρ, C_P, k values of the PVA electrolyte, carbon electrode and conventional external scaffold (Al foil) are 1.2×10^3, 1.2×10^7, 0.03; 1.4×10^3, 1.4×10^3, 1.04; and 2.7×10^3 kg m^{-3}, 0.9×10^3 J kg^{-1} K^{-1}, 238 W m^{-1} K^{-1}, respectively.[19,20]

Characterization

Cyclic voltammetry (CV) was carried out at various current levels using a computer-controlled potentiostat (Zive sp2, Zive Lab). The specific capacitance (F g^{-1}), C_{sp}, was calculated from the CVs according to the following equation:

$$C_{sp} = \frac{\int_{V_i}^{V_f} I/(v \times m) dV}{(V_f - V_i)} \quad (5)$$

where I is the current (A), v is the scan rate (V s^{-1}), m is the mass of the electrodes (g) and $V_f - V_i$ is the potential window (V). CVs were conducted under harsh conditions, such as bending and stretching states, to evaluate the mechanical stability. The morphologies of the CNT–graphene layered electrodes were observed with scanning electron microscopy (SEM, Sigma, Carl Zeiss).

Gas permeability measurements

CO_2 gas was employed to examine the selective gas permeable property of the external GPE film in this study. The external GPE was fixed between a hollow bolt and a cap closing the end of the flow line. The line starts from the pressure gauge that is connected to a CO_2 tank. An initial pressure of 1.5 bar was applied to the PVA film, and pressure reduction was monitored as a function of time.

Results and discussion

To fabricate a prototype device with an endoskeleton, we fully developed our previous research for unconventional energy storage architectures.[15–18,21] Here, we show a concrete example of a prototype device with an endoskeleton as a capacitive energy storage device using an electrical double layer (EDL). The EDL capacitor is one of the more promising energy storage devices for the next generation because of its unique properties, including a variety of fabrication methods, wide range of operating temperatures, and safety.[15,18] The strategy proposed here, however, can be easily extended to other types of energy storage (*e.g.*, lithium or sodium ion batteries) by further studies.[9,13] The porous and internal scaffold (the endoskeleton) was fabricated using polypropylene sheets that were used as the substrate of an origami-type energy storage device (see Experimental section and Fig. S2†).[17] The sheets play roles not only as a skeleton but also as an ion transferring substrate. In terms of mechanical properties, the system shows stable foldability, which is a common characteristic of conventional sheets.[17] The electrodes of the system were composed of graphene and carbon-nanotubes (CNT) in the form of a layered structure (Fig. S1†). In this electrode, graphene serves as an active site and as a floating track on the CNTs. CNT clusters, a conducting material, convert external stress into the stretching motion of the electrode, as reported in our previous research.[15] From this mechanism, the electrode system shows multifunctionality, such as omnidirectional stretching and energy storage by the formation of a large surface EDL.[15]

To realize an endoskeleton system, the solid electrolyte is a critical component. As an external skin, the electrolyte should have sufficient strength and flexibility. In this system, we used a PVA-based gel polymer electrolyte (GPE), which has non-toxic, non-carcinogenic, bioadhesive and viscoelastic characteristics.[22] Based on these characteristics, the material has been used as an artificial skin and in drug-delivery applications.[22] PVA has a dynamic modulus of 80 MPa and a tensile yield strength of 23 MPa, which confer an appropriate strength and a high degree of stretchability.[23] In addition, these values are quite similar to those of human skin,[24] suggesting that the final system could be applicable for use as an external layer in human integrated electronics.[25] Specifically, PVA/H_3PO_4 was used as a GPE because of the fast charge transport *via* the large overlapping polaron tunneling (OLPT) of ions inside the PVA chains.[26]

The schematics of the endoskeleton and conventional systems for energy storage are shown in Fig. 2. In the case of a conventional (exoskeleton) system, the main components, including a passive scaffold, electrodes, and an electrolyte, are stacked from the outside to the inside.[7] On the other hand, the order of the stacked structures in an endoskeleton system is completely opposite of that for conventional systems. The passive scaffold is the most rigid part of an energy storage architecture and has a lower elasticity compared to the other parts. In a conventional system, the rigidity of the systems decreases from the outside to the inside, which indicates that a mechanically neutral plane (a counterbalanced region between opposite strains) makes up the most flexible component in the system (Fig. 2a).[27] In a bending state of conventional systems, tensile and compressive strains arise in the outer and inner sides, respectively. As a consequence, opposing forces can easily cause defects in the systems because of a difference in strains on the top and bottom scaffolds (Fig. S3†). On the other hand, rigid scaffolds are located on a mechanically neutral plane in endoskeleton systems, and the flexibility in the system is unlimited, the only consideration is the depth of the inner passive scaffold (Fig. 2b). In this system, an optimized configuration is not required to minimize the potential for mechanical fracture because the structure of the device is orthogonally symmetrical from the rigid middle plane. In previously reported techniques, flexibility can be introduced by the use of stretchable materials[8,11] or serpentine arrays.[9,10] However, all such architectures are comprised of external scaffolds, which inevitably results in the imposition of mechanical limitations to the system, such as flexible properties.

The prototype endoskeleton has good foldability, but its stretchability is limited. The tensile modulus and strain to failure for this material are 15 GPa and 7%.[28] To assign a stretching property to the device, pores can be located hexagonally in the scaffold, resulting in serpentine networks along the x–y plane (Fig. 3a). There are three serpentine lines in different directions on the two dimensional scaffold, and the lines appear at an interval of $\pi/3$ radian. The serpentine lines permit omni-directional stretching to be possible. Under 15% uniaxial-stretching, the average equivalent strain on the endoskeleton system is only 7%. This value is quite small in

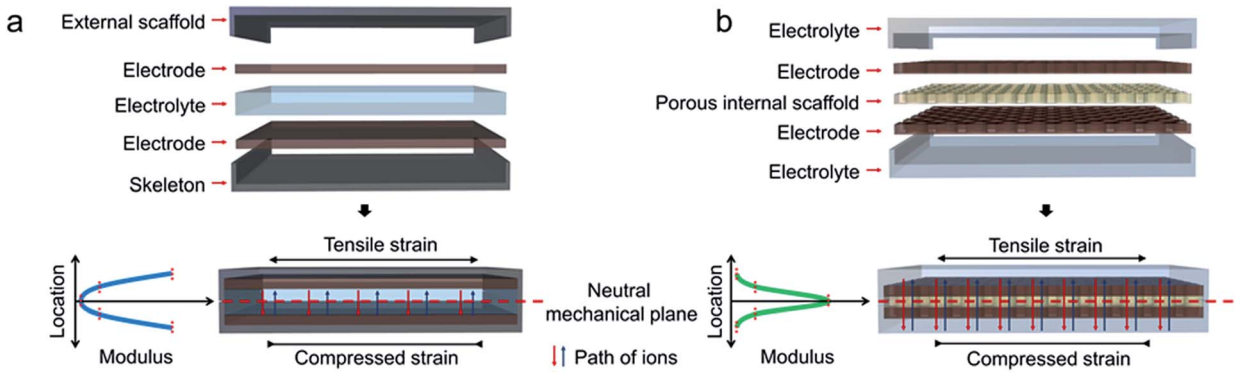

Fig. 2 An exoskeleton energy storage system *versus* an endoskeleton energy storage system. (a and b) Schematic of (a) an exoskeleton energy storage system and (b) an endoskeleton energy storage system. Inset plots are *y* directional relative location *versus* modulus in the two systems.

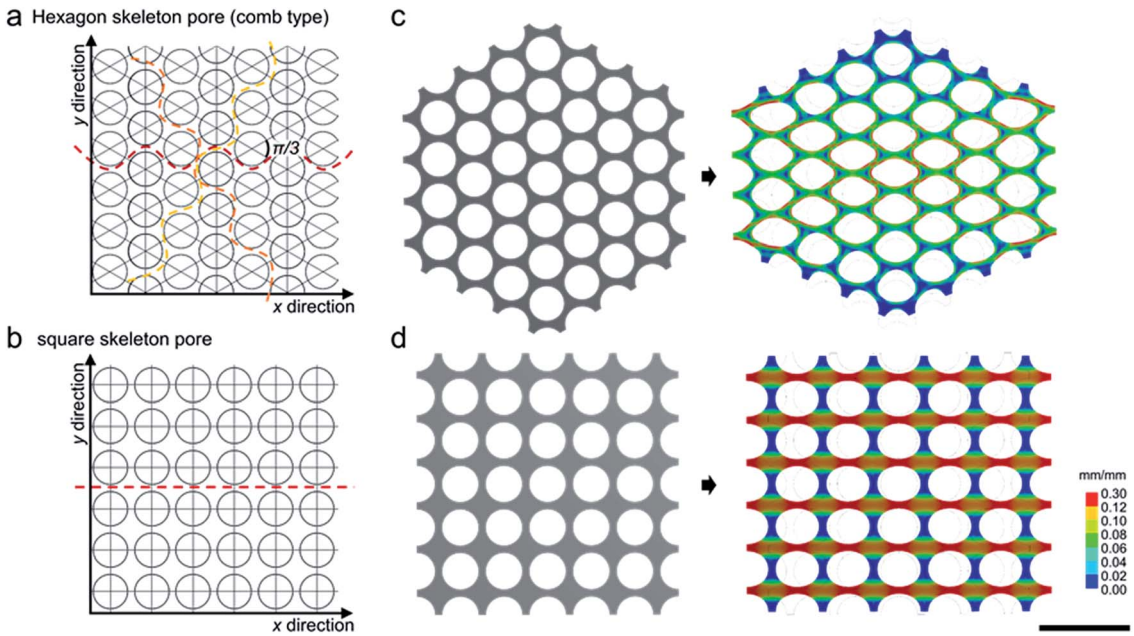

Fig. 3 Stretching properties of endoskeletons with pore structure. (a and b) Schematic of (a) hexagonally located pores and (b) tetragonally located pores. (c and d) Equivalent strains of the endoskeleton with (c) hexagonal skeleton pores and (d) square skeleton pores for stretching deformation (15%) by a finite element model calculation. (c) In the hexagon skeleton pores, there are three serpentine lines with different directions in the two dimensional scaffold, and the lines appear at an interval of π/3 radian. Scale bar is 10 mm.

comparison with the strain of a sheet without pores or with tetragonally placed pores (the average strain is 15%) (Fig. 3b–d). The above findings indicate that the hexagonally-located pore structure can result in minimized strain and stress, and that the system is stable during deformation as the result of stretching.

Fig. 4 shows the cyclic voltammograms of the endoskeleton system with the graphene layered electrodes at various deformation states. In the un-deformed state, the specific capacitances (C_{sp}) were found to be 130, 82 and 61 F g^{-1} for scan rates of 0.1, 0.3 and 0.5 mV s^{-1}, respectively, based on the mass of the active component, which is similar to the performance of conventional carbon allotrope electrodes with external scaffolds.[29] Based on the C_{sp}s, we also show a Ragone plot for the endoskeleton system (Fig. S4†). The specific energy and power are around 10 W h kg^{-1} and 10–20 W kg^{-1}, respectively. These values are the same general values for an electric double layer capacitor system using carbon allotrope electrodes and aqueous electrolytes with an external scaffold in previous research.[30–32] On the other hand, the volume and the density of the endoskeleton (*i.e.*, polypropylene, 855 kg m^{-3}) are significantly lower than that of the exoskeletons, which is similar to metal covers on coin cells or laminated covers in pouch types (*i.e.*, stainless steel, ~8000 kg m^{-3}). This means that the electrochemical properties based on the mass of the cell are significantly improved when an endoskeleton configuration is adopted. A simple application to devices on the human body (a wrist) is shown in Fig. 4d. The system on the skin is sufficiently flexible and light.

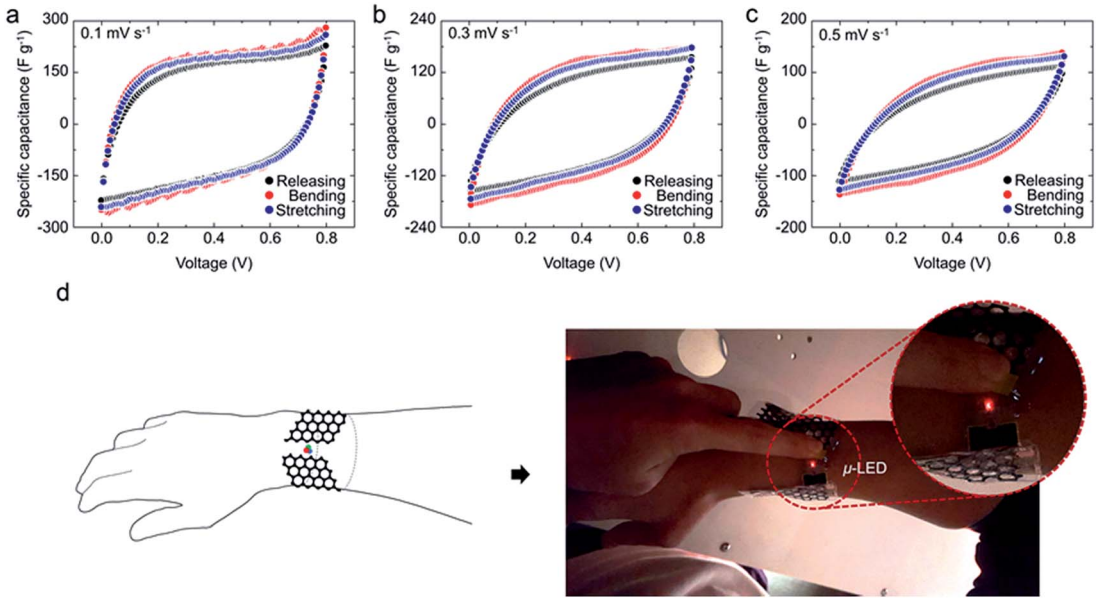

Fig. 4 Electrochemical analyses of the endoskeleton system. Representative cyclic voltammetry curves at various scan rates without strain (black dots) and with bending (bending radius, 0.5 mm; red dots) and stretching (15%; blue dots). Scan rates were (a) 0.1, (b) 0.3, (c) 0.5 mV s^{-1}. (d) An application of the endoskeleton system in a micro-LED device on human body (a wrist).

The system exhibited excellent capacitance stability under folding and stretching conditions. Even an increase in C_{sp} was observed when a flat system was deformed. In the deformation state for bending (bending radius 0.5 mm, Fig. S5a†), C_{sp} values of 154, 106 and 83 F g^{-1} were achieved at scan rates of 0.1, 0.3 and 0.5 mV s^{-1}, respectively. In the case of 15% stretching (Fig. S5b†), the C_{sp} values were 144, 95 and 73 F g^{-1}, which is also consistent with the galvanostatic charge/discharge analyses (C/Ds) (Fig. S6†). The coulombic efficiency reaches about 90% regardless of the deformation states, which indicates good reversibility of the electrochemical performances. These results can be attributed to the fact that the bending and stretching of the electrolyte induces pressure from the electrolyte membrane on the skeleton, thus creating a closer interaction between the electrolyte membrane and the electrodes, as reported in previous research.[15,18] Stability is an important parameter for evaluating the suitability of devices for practical applications. Fig. S7† shows the cycling stability of the energy storage device with an endoskeleton. The structure showed good cyclic stability, and it maintained a capacitance of ~100% of the original value at the initial cycle, even after 400 cycles. To demonstrate the mechanical stability, the CVs of the energy storage device with an endoskeleton were examined after 50 bending/releasing and 50 stretching/releasing cycles (Fig. S8†). Compared to a CV curve before deformation, the C_{sp} values were maintained at over 97 and 90%, respectively, which proves that the system shows consistent electrochemical and mechanical performance.

The main reason for unsafe conditions in an energy storage device is that the generation of gas can cause a sudden release of flammable solvent vapours, which can lead to an explosive fuel–air mixture being produced. Therefore, large-scale exoskeleton systems require a designed venting module that allows gas to be released to the external environment.[33] The permeability of O_2 through the PVA membrane is less than 5 cm^3 m^{-2} per day.[34] Considering that the values for the BOPP and PET films are about 2500 and 150 cm^3 m^{-2} per day, the O_2 permeability of PVA is negligible.[34] Therefore, the PVA membrane covering the external of the endoskeleton systems can serve as an O_2 barrier and also protect the cell from atmospheric attack as conventional external scaffolds do. However, PVA has a relatively high CO_2 permeability with a high selectivity.[35] CO_2 is the largest portion of gas evolved inside conventional energy storage cells.[33,36] The PVA membrane permits an internal gas (such as CO_2) to diffuse out of the cell. Even though PVA–H_3PO_4 GPE does not include a flammable solvent, the breathing property of the gel-polymer external skin prevents high pressures from developing inside the cell, which consequently significantly improves safety. To investigate gas diffusion properties through a GPE external layer, closed systems with a GPE, an external skin in the endoskeleton system, and an Al surface, an external scaffold in conventional system, were fabricated with a pressure difference of CO_2 gas (1.5 bar) between the inside and outside surfaces. The conventional Al metal external scaffold immediately collapsed as a result of the pressure difference, which can cause the system to explode (Fig. S9†). On the other hand, the GPE layer was stable, resisted the relatively high pressure, and maintained an inflated state (Fig. 5). The relative pressure in the closed packing system with the GPE surface decreased exponentially, which means that continuous gas diffusion occurred through the GPE external cover (Fig. S10†). This result proves that an endoskeleton system with a GPE skin has a high level of safety.

A high rate of gas generation accompanies thermal runaway, which is the most important concern regarding the safety of energy storage devices. For example, the alkyl carbonate-based

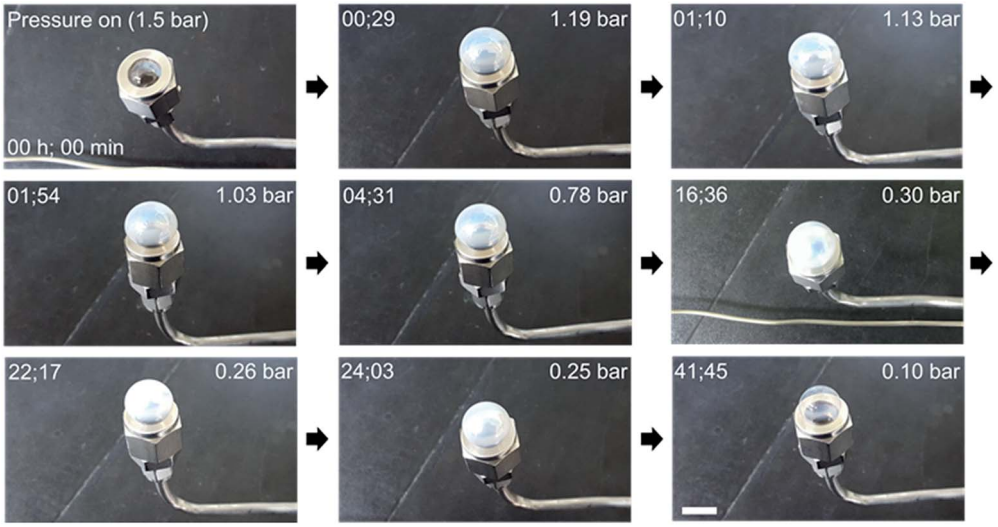

Fig. 5 States of the PVA–H_3PO_4 gel polymer electrolyte (GPE) skin with CO_2 pressure difference between the surfaces. The deformation state of PVA–H_3PO_4 GPE at various times. Scale bar is 1 cm. Scale bar is 10 mm.

electrolyte used for secondary batteries exhibits a breakdown at elevated temperatures of around 423–473 K.[33] The heat in energy storage cells is generated on electrode materials during the charge–discharge process because the resistance of materials cannot be completely eliminated (emitted thermal energy, $E = I^2Rt$). In a conventional system, the external scaffolds, which are in contact with the electrode, have a low specific heat, resulting in the electrolyte having a high local temperature. The scaffolds operate as a heating box and release heat toward the overall electrolyte. The temperature causes gas to be produced in the electrolyte, and the resulting gas causes an explosion as a chain-reaction. In endoskeleton systems, the GPE covering interfaces directly with the environment, and the electrode allows the heat in the electrolyte to diffuse out to the environment. The three-dimensional finite element method was used in analysing the temperature of the two systems, and the results are shown in Fig. S11.† The electrolyte in the exoskeleton that is over-heated omni-directionally represents high temperature conditions that are susceptible to the formation of gas. On the other hand, the temperature of an electrolyte constituting an endoskeleton structure was maintained at a low-level.

Conclusion

In conclusion, we reported on a new branch of evolution for energy storage devices. An energy storage device composed of an endoskeleton has three important advantages: (1) flexibility, (2) a small volume of passive structure and (3) gas and heat readily diffuse. This features are currently taking centre stage in the field of energy storage. The prototype still has drawbacks, such as relatively low ion diffusion and weak strength, that must be resolved for practical applications. However, this research includes a unique breakthrough to address problems associated with the use of external scaffolds, which has not been considered until now.

Acknowledgements

This research was supported by the Global Frontier R&D Program on Centre for Multiscale Energy System funded by the National Research Foundation under the Ministry of Science, ICT & Future, Republic of Korea (NRF-2011-0031571).

References

1 S. J. Gould, *J. Hist. Biol.*, 1970, **3**, 189–212.
2 D. A. J. Rand, *J. Solid State Electrochem.*, 2011, **15**, 1579–1622.
3 X. Wang, X. Lu, B. Liu, D. Chen, Y. Tong and G. Shen, *Adv. Mater.*, 2014, **26**, 4763–4782.
4 T.-H. Kim, J.-S. Park, S. K. Chang, S. Choi, J. H. Ryu and H.-K. Song, *Adv. Energy Mater.*, 2012, **2**, 860–872.
5 B. Dunn, H. Kamath and J.-M. Tarascon, *Science*, 2011, **334**, 928–935.
6 C. H. Kennedy, *J. Morphol.*, 1927, **44**, 267–312.
7 R. Wagner, N. Preschitschek, S. Passerini, J. Leker and M. Winter, *J. Appl. Electrochem.*, 2013, **43**, 481–496.
8 Z. Song, T. Ma, R. Tang, Q. Cheng, X. Wang, D. Krishnaraju, R. Panat, C. K. Chan, H. Yu and H. Jiang, *Nat. Commun.*, 2014, **5**, 3140.
9 S. Xu, Y. Zhang, J. Cho, J. Lee, X. Huang, L. Jia, J. A. Fan, Y. Su, J. Su, H. Zhang, H. Cheng, B. Lu, C. Yu, C. Chuang, T. Kim, T. Song, K. Shigeta, S. Kang, C. Dagdeviren, I. Petrov, P. V. Braun, Y. Huang, U. Paik and J. A. Rogers, *Nat. Commun.*, 2013, **4**, 1543.
10 G. Lee, D. Kim, D. Kim, S. Oh, J. Yun, J. Kim, S.-S. Lee and J. S. Ha, *Energy Environ. Sci.*, 2014, **8**, 1764–1774.
11 Z. Niu, H. Dong, B. Zhu, J. Li, H. H. Hng, W. Zhou, X. Chen and S. Xie, *Adv. Mater.*, 2013, **25**, 1058–1064.
12 J. Ren, Y. Zhang, W. Bai, X. Chen, Z. Zhang, X. Fang, W. Weng, Y. Wang and H. Peng, *Angew. Chem., Int. Ed.*, 2014, **53**, 7864–7869.

13 J. Ren, W. Bai, G. Guan, Y. Zhang and H. Peng, *Adv. Mater.*, 2013, **25**, 5965.
14 X. Chen, L. Qiu, J. Ren, G. Guan, H. Lin, Z. Zhang, P. Chen, Y. Wang and H. Peng, *Adv. Mater.*, 2013, **25**, 6436.
15 I. Nam, S. Bae, S. Park, Y. G. Yoo, J. M. Lee, J. W. Han and J. Yi, *Nano Energy*, 2015, **15**, 33–42.
16 I. Nam, J. Park, S. Park, S. Bae, Y. G. Yoo and J. Yi, *Adv. Energy Mater.*, 2016, **6**, 1501812.
17 I. Nam, G.-P. Kim, S. Park, J. W. Han and J. Yi, *Energy Environ. Sci.*, 2014, **7**, 1095–1102.
18 I. Nam, S. Park, G.-P. Kim, J. Park and J. Yi, *Chem. Sci.*, 2013, **4**, 1663–1667.
19 M. I. Abdel-Ati, O. M. Hemeda, M. M. Mosaad and D. M. Hemeda, *J. Therm. Anal.*, 1994, **42**, 1113–1122.
20 S. C. Chen, C. C. Wan and Y. Y. Wang, *J. Power Sources*, 2005, **140**, 111–124.
21 I. Nam, G.-P. Kim, S. Park, J. Park, N. D. Kim and J. Yi, *Nanoscale*, 2012, **4**, 7350–7353.
22 C. M. Hassan and N. A. Peppas, *Adv. Polym. Sci.*, 2000, **153**, 37–65.
23 W.-I. Cha, S.-H. Hyon, M. Oka and Y. Ikada, *Macromol. Symp.*, 1996, **109**, 115–126.
24 P. G. Agache, C. Monneur, J. L. Leveque and J. D. Rigal, *Arch. Dermatol. Res.*, 1980, **269**, 221–232.
25 C. Dagdeviren, Y. Shi, P. Joe, R. Ghaffari, G. Balooch, K. Usgaonkar, O. Gur, P. L. Tran, J. R. Crosby, M. Meyer, Y. Su, R. C. Webb, A. S. Tedesco, M. J. Slepian, Y. Huang and J. A. Rogers, *Nat. Mater.*, 2015, **14**, 728–736.
26 M. Z. Kufian, S. R. Majid and A. K. Arof, *Ionics*, 2007, **13**, 231–234.
27 D.-H. Kim, J.-H. Ahn, W. M. Choi, H.-S. Kim, T.-H. Kim, J. Song, Y. Y. Huang, Z. Liu, C. Lu and J. A. Rogers, *Science*, 2008, **320**, 507–511.
28 B. Alcock, N. O. Cabrera, N.-M. Barkoula, C. T. Reynolds, L. E. Govaert and T. Peijs, *Compos. Sci. Technol.*, 2007, **67**, 2061–2070.
29 L. L. Zhang and X. S. Zhao, *Chem. Soc. Rev.*, 2009, **38**, 2520–2531.
30 D. P. Dubal, O. Ayyad, V. Ruiz and R. Gómez-Romero, *Chem. Soc. Rev.*, 2015, **44**, 1777–1790.
31 S.-E. Chun, B. Evanko, X. Wang, D. Vonlanthen, X. Ji, G. D. Stucky and S. W. Boettcher, *Nat. Commun.*, 2015, **6**, 7818.
32 P. Simon and Y. Gogotsi, *Nat. Mater.*, 2008, **7**, 845–854.
33 E. P. Roth and C. J. Orendorff, *Electrochem. Soc. Interface*, 2012, 45–49.
34 J.-H. Yeun, G.-S. Bang, B. J. Park, S. K. Ham and J.-H. Chang, *J. Appl. Polym. Sci.*, 2006, **101**, 591–596.
35 Y. Cai, Z. Wang, C. Yi, Y. Bai, J. Wang and S. Wang, *J. Membr. Sci.*, 2008, **310**, 184–196.
36 A. Wuersig, W. Scheifele and P. Novák, *J. Electrochem. Soc.*, 2007, **154**, A449–A454.

